REGULAR ARTICLE

blood advances

Comparing the value of mono- vs coculture for high-throughput compound screening in hematological malignancies

Sophie A. Herbst,[1-5,*] Vladislav Kim,[2,3,5,*] Tobias Roider,[1-3,*] Eva C. Schitter,[1] Peter-Martin Bruch,[1-3,6] Nora Liebers,[1-4] Carolin Kolb,[1] Mareike Knoll,[1] Junyan Lu,[2,3] Peter Dreger,[1] Carsten Müller-Tidow,[1-3] Thorsten Zenz,[7] Wolfgang Huber,[2,3,†] and Sascha Dietrich[1-3,6,†]

[1]Department of Medicine V, Hematology, Oncology and Rheumatology, Heidelberg University Hospital, Heidelberg, Germany; [2]Genome Biology Unit, European Molecular Biology Laboratory, Heidelberg, Germany; [3]Molecular Medicine Partnership Unit, Heidelberg, Germany; [4]Department of Translational Medical Oncology, National Center for Tumor Diseases Heidelberg, German Cancer Research Center (DKFZ), Heidelberg, Germany; [5]Faculty of Biosciences, University of Heidelberg, Heidelberg, Germany; [6]Department of Hematology and Oncology, University Hospital Düsseldorf, Düsseldorf, Germany; and [7]Department of Medical Oncology and Hematology, University Hospital Zürich, Zürich, Switzerland

Key Points

- Stromal coculture mediates resistance to various drug classes, including chemotherapeutics, B-cell receptor, proteasome, and BET inhibitors.
- Detected drug-gene associations agreed between mono- and coculture but effect sizes and number of discoveries were higher in monoculture.

Large-scale compound screens are a powerful model system for understanding variability of treatment response and discovering druggable tumor vulnerabilities of hematological malignancies. However, as mostly performed in a monoculture of tumor cells, these assays disregard modulatory effects of the in vivo microenvironment. It is an open question whether and to what extent coculture with bone marrow stromal cells could improve the biological relevance of drug testing assays over monoculture. Here, we established a high-throughput platform to measure ex vivo sensitivity of 108 primary blood cancer samples to 50 drugs in monoculture and coculture with bone marrow stromal cells. Stromal coculture conferred resistance to 52% of compounds in chronic lymphocytic leukemia (CLL) and 36% of compounds in acute myeloid leukemia (AML), including chemotherapeutics, B–cell receptor inhibitors, proteasome inhibitors, and Bromodomain and extraterminal domain inhibitors. Only the JAK inhibitors ruxolitinib and tofacitinib exhibited increased efficacy in AML and CLL stromal coculture. We further confirmed the importance of JAK-STAT signaling for stroma-mediated resistance by showing that stromal cells induce phosphorylation of STAT3 in CLL cells. We genetically characterized the 108 cancer samples and found that drug-gene associations strongly correlated between monoculture and coculture. However, effect sizes were lower in coculture, with more drug-gene associations detected in monoculture than in coculture. Our results justify a 2-step strategy for drug perturbation testing, with large-scale screening performed in monoculture, followed by focused evaluation of potential stroma-mediated resistances in coculture.

Introduction

Ex vivo compound screening has improved our understanding of the phenotypic and molecular heterogeneity of tumor diseases.[1-10] In patients with hematological malignancies, profiling drug responses

Submitted 19 January 2023; accepted 7 June 2023; prepublished online on *Blood Advances* First Edition 23 June 2023. https://doi.org/10.1182/bloodadvances.2022009652.

*S.A.H., V.K., and T.R. contributed equally to this study.

†W.H. and S.D. are joint senior authors and contributed equally to this study.

Primary imaging data were deposited to the Image Data Resource (https://idr.openmicroscopy.org) under accession number idr0143. Raw and normalized drug response data of mono- and coculture are available on GitHub (https://github.com/vladchimescu/coculture.git).

The full-text version of this article contains a data supplement.

on demand has even been demonstrated to support clinical decision making by suggesting personalized treatment options.[11,12] The disadvantage that most of these studies face is that, deprived of microenvironmental stimuli, leukemia cells undergo spontaneous apoptosis ex vivo.[13,14] There are several approaches for modeling the leukemia microenvironment ex vivo, for instance, by adding conditioned medium from stromal cells[15,16] or by providing specific stroma-secreted cytokines.[17] However, not only soluble factors, but also the direct contact with stromal cells play an essential role in promoting the survival of leukemia cells in the bone marrow.[18] Coculture studies revealed that bone marrow–derived stromal cells protect leukemia cells even from drug-induced apoptosis,[19-22] which may contribute to residual disease[23] and the emergence of resistant clones.[24] Therefore, stroma-leukemia coculture models are considered a potential ex vivo platform to profile drug responses of tumor cells while mimicking the interactive effects of the microenvironment.[10,20,25-27]

Although coculture models appear more natural to profile drug response ex vivo, given the complexity and extra effort to establish and read out such a model, the application must be carefully considered. Unfortunately, the validity of coculture models has not been tested rigorously, and current evidence is limited to individual compounds probed in small-scale coculture studies.[19-21,28-35]

To systematically assess whether coculture studies provide superior biological insights, we performed a large-scale study comparing compound efficacy in leukemia monoculture and leukemia-stroma coculture. We used the well-established bone marrow–derived stroma cell line HS-5 and an imaging-based platform to investigate not only drug effects in monoculture and leukemia-stroma coculture but also to capture cellular changes because of the stromal environment and drug treatments. Finally, we suggest a 2-stage strategy of high-throughput drug perturbation in monoculture, followed by targeted evaluation of stroma-mediated resistance in cocultures.

Materials and methods

Cell culture

HS-5 cells were cultured in Dulbecco's modified Eagle medium (DMEM; Thermo Fisher Scientific) supplemented with 10% fetal bovine serum (FBS; Thermo Fisher Scientific), 1% penicillin/streptomycin (Thermo Fisher Scientific), and 1% glutamine (Thermo Fisher Scientific) in a humidified atmosphere at 37°C and 10% CO_2.

Patient samples

Written consent was obtained from all patients according to the Declaration of Helsinki. In addition, our study was approved by the ethics committee of the University of Heidelberg. Samples were selected based on availability and tumor cell content >80%. Clinical flow cytometry data were used to estimate the proportion of malignant cells in the collected blood samples. Peripheral blood mononuclear cells were isolated using Ficoll density gradient centrifugation. Cells were viably frozen in RPMI (Thermo Fisher Scientific) containing 45% FBS (Thermo Fisher Scientific) and 10% dimethyl sulfoxide (DMSO; SERVA Electrophoresis GmbH) and kept on liquid nitrogen until use. Cells were thawed freshly before the experiment and rolled in serum-containing medium for 3 hours on a roll mixer at room temperature to allow cells to recover. To deplete dead cells, which form clumps during this procedure, the suspension was filtered through a 40 μm cell strainer (Sarstedt). Cell viability and counts were analyzed using trypan blue (Thermo Fisher Scientific). Percentages of alive cells always exceeded 90% at culture start or freezing of pellets.

IGHV status analysis

For the analysis of immunoglobulin heavy chain variable region (IGHV) status, RNA was isolated from 1×10^7 peripheral blood mononuclear cells, and complementary DNA was synthesized via reverse transcription. Subsequent polymerase chain reactions and analyses were performed according to the method of Szankasi and Bahler, with minor modifications.[36] A detailed description can be found in the supplemental Methods of this manuscript.

Panel sequencing of CLL samples

We performed an analysis of gene mutations of the chronic lymphocytic leukemia (CLL) candidate genes NOTCH1, SF3B1, ATM, TP53, RPS15, BIRC3, MYD88, FBXW7, POT1, XPO1, NFKBIE, EGR2, and BRAF. A detailed description of the analysis can be found in the supplemental Methods of this manuscript.

DNA copy number variants

Assessment of DNA copy numbers was done using Illumina CytoSNP-12 and HumanOmni2.5-8 microarrays and read out using an iScan array scanner. Fluorescence in situ hybridization analysis was performed for del11q22.3, del17p13, del13q14, trisomy 12, gain8q24, and gain14q32. Only alterations present in ≥3 patients and absent in ≥3 patients were considered.

Drug plate preparation

For the screen, 50 drugs were probed at 3 different concentrations (supplemental Table 1). Drug concentrations ranged from subnanomolar to low micromolar and were chosen based on previous experience with the drugs.[3] Increase of the concentration was 15-fold per step to cover a broad spectrum of concentrations. Drugs were diluted according to the manufacturer instructions. Further dilution was carried out in DMSO (SERVA Electrophoresis GmbH), and master plates containing 4 μL of diluted drugs were frozen at −20°C for direct use on the screening days.

Compound screening of monocultures and cocultures

Drug screens were carried out in CellCarrier-384 Ultra Microplates (Perkin Elmer) with a seeding density of HS-5 stromal cells of 1×10^4 cells per well and 2×10^4 patient cells per well. The screen was carried out in DMEM; Thermo Fisher Scientific) supplemented with 10% human serum (male AB, H6914-100ml Batch SLBT2873, Sigma-Aldrich), 1% penicillin/streptomycin (Thermo Fisher Scientific), and 1% glutamine (Thermo Fisher Scientific) at a final volume of 40 μL in the culture plates. Cells were incubated at 37°C in a humidified atmosphere and 10% CO_2 for 3 days. A detailed description of the screen can be found in the supplemental Methods section.

Staining and spinning disk confocal microscopy

High-throughput screening was conducted using Opera Phenix High Content Screening System (Perkin Elmer). CLL screening plates were stained with 4 μg/mL Hoechst 33342 (Invitrogen) and 1

μL/mL lysosomal dye NIR (Abcam). Plates of non-CLL entities were additionally stained with 1 μM Calcein AM (Invitrogen). All dyes were diluted using serum-free medium and staining solution was added to each well. After an incubation period of 45 minutes at 37°C, 3 positions per well with a stack of 10 images at a distance of 1.2 μm were acquired with a 40× water objective in confocal mode.

Primary mesenchymal stromal cells (MSCs) cocultures

Drug screen results for 1.5 μM JQ1, 0.6 μM Fludarabine, 22.5 μM tofacitinib, and 9 μM ruxolitinib were validated in cocultures with primary MSCs derived from 3 different healthy donors. Each condition was assessed in technical duplicates. For a detailed description, refer to the supplemental Methods of this manuscript.

Processing of images (CLL)

Images of CLL samples were processed using the image analysis software Harmony (Perkin Elmer). Results were further analyzed in the statistical programming language R (R Core Team, 2018). For a detailed description, see the supplemental Methods of this manuscript.

Image analysis in non-CLL entities

Maximum intensity projection and gamma correction ($\gamma = 0.3$) was applied to all images. All 3 color channels (lysosomal dye, Calcein, and Hoechst) were combined to generate RGB (red, green, blue) overlays. Each image (2160 × 2160, omitting the color channel axis) was cut into 9 blocks of size 720 × 720 to speed up training and prediction.

Faster Region-based Convolutional Neural Network (R-CNN) object detection model[37] with Inception v2[38] backbone architecture was used to detect leukemia and lymphoma cells derived from patients. The 2 defined classes were viable and apoptotic leukemia cells. The object detection model implemented in TensorFlow 1.14 was trained for 21 000 epochs on coculture images from 5 acute myeloid leukemia (AML) samples. A total of 5 control and 5 drug-treated well images were randomly selected from each of the 5 AML plates, resulting in 5 × 10 × 9 = 450 images that were split into train/test sets with 80%/20% ratio. The average precision on the test set was 0.99 and 0.93 for viable and apoptotic leukemia cells, respectively. The area under the receiver operating characteristic curve was 0.98 for both viable and apoptotic leukemia cells.

Identification of conditions toxic to stromal cells

Drug concentrations that were toxic to stroma cells were excluded, as these do not represent proper cocultures. The degree of stroma cell death was assessed by evaluating the percentage of area covered by stroma cells using the image analysis software Harmony (Perkin Elmer). For this, all nuclei were segmented in the Hoechst channel and CLL nuclei were excluded by setting a size threshold. Next, the cytoplasm of stroma cells was found using the signal from the lysosomal dye as proxy. Conditions in which <40% of the image area was covered by stroma were classified as toxic conditions.

Morphological profiling, quality control, and normalization

After image segmentation, morphological properties describing size, intensity, shape, and texture were computed for each cell. Morphological profiling of leukemia cells derived from patients produced 1401 image features in non-CLL entities and 934 features in CLL. In all downstream analyses, we used only a subset of features with high replicate correlation ($r > 0.5$). After filtering based on replicate correlation, we obtained 173 morphological features in non-CLL entities and 194 features in CLL. All morphological properties were normalized to control values. Mean and standard deviation of each image feature were estimated using untreated wells in monoculture and coculture, respectively. All morphological features were centered and scaled:

$$x_{norm} = \frac{x - \mu_M}{\sigma_M} \text{ monoculture}$$

$$x_{norm} = \frac{x - \mu_C}{\sigma_C} \text{ coculture}$$

Spontaneous apoptosis, drug sensitivity and normalization

Only viable and apoptotic leukemia cell counts were used for drug sensitivity analysis. Viability was computed as the ratio of viable cell count to the total cell count. For each sample, baseline viabilities (b_M, b_C) were defined as mean viabilities of untreated wells of the respective culture condition. Untreated wells on the plate edge were excluded, resulting in 11 and 13 wells used for estimation of baseline viability in monoculture and coculture, respectively. Spontaneous apoptosis rate was evaluated as the complement of baseline viability:

$$SA = 1 - b.$$

Drug sensitivities were computed by normalizing viabilities to baseline values of the respective culture condition:

$$\nu_{norm} = \frac{\nu}{b_M} \text{ monoculture}$$

$$\nu_{norm} = \frac{\nu}{b_C} \text{ coculture}$$

Compound efficacy changes in coculture

For each drug, we selected the concentration with maximum variance in terms of normalized viability and applied a paired t test with the null hypothesis H_0 assuming equal drug sensitivities in monoculture and coculture. Drug concentrations toxic to stromal cells were excluded before statistical testing but were retained for dose-response fitting.

To compute the effect size, median dose-response curves were computed for monoculture and coculture. The effect size was calculated as the percentage change in area under the dose-response curves in coculture:

$$\text{Effect size} = \frac{AUC_C - AUC_M}{AUC_M} \cdot 100\%$$

In CLL coculture, compounds with changed efficacy had adjusted P values of <.01 and |effect size| >5%. In AML coculture, the same thresholds were used, except for those compounds that change efficacy in CLL coculture, for which only the effect size cutoff of 5% was used.

Drug-gene associations

For 80 CLL samples, genetic features such as IGHV mutation status, somatic mutations (TP53, ATM, etc), and chromosomal aberrations (del11q, trisomy 12, etc) were available. To test whether mean drug sensitivities of wildtype and mutated cases were equal, we applied a *t* test on normalized viabilities for each drug stratified by mutational status. The statistical tests were performed separately in monoculture and coculture.

Western blot analysis

To assess the impact of stroma coculture on STAT3 phosphorylation in CLL cells, DMEM medium supplemented with 10% human serum (male AB, H6914-100ml Batch SLBT2873, Sigma-Aldrich), 1% penicillin/streptomycin (Thermo Fisher Scientific), and 1% glutamine (Thermo Fisher Scientific) or 5×10^6 HS-5 cells were preplated into 10 cm dishes. After 3 hours, CLL cells were added at 1.5×10^7 cells per dish to establish monocultures and cocultures. DMSO (0.22%; SERVA Electrophoresis GmbH), ruxolitinib (10 μM), or tofacitinib (22 μM) were added. After incubation for 48 hours, CLL cells were carefully harvested. Cells were counted using trypan blue (Thermo Fisher Scientific), and contamination with HS-5 cells was excluded by visual inspection. To assess the impact of soluble factors produced by stroma, HS-5 cells or primary MSCs were cultured in DMEM medium supplemented with 10% FBS (Thermo Fisher Scientific), 1% penicillin/streptomycin (Thermo Fisher Scientific), and 1% glutamine (Thermo Fisher Scientific) or Bulletkit medium (Lonza). Conditioned medium was harvested after 3 days of culture. After the removal of cellular debris by centrifugation at 1000*g*, aliquots of conditioned medium were frozen. A total of 7.5×10^6 CLL cells derived from patients with CLL in DMEM medium supplemented with 10% FBS (Thermo Fisher Scientific), 1% penicillin/streptomycin (Thermo Fisher Scientific), 1% glutamine (Thermo Fisher Scientific), and 25% conditioned medium were seeded into 10 cm dishes. Cells were harvested after culturing for 48 hours. Western Blot was performed using the primary antibodies anti-phospho-STAT3^{Tyr705} (Cell Signaling Technology, #9145), anti-STAT3 (Cell Signaling Technology, #30835), anti-β-actin (Proteintech Group, #66009-1-Ig), and the secondary antibodies, anti-mouse–immunoglobulin G–horseradish peroxidase–conjugated (Proteintech Group, #SA00001-1) and anti-rabbit–immunoglobulin G–horseradish peroxidase–conjugated (Proteintech Group, #SA00001-2). A detailed description of the protocol can be found in the supplemental Methods of this manuscript.

Software availability

Image analysis and morphological profiling were conducted in Python and the code is available on Github (https://github.com/vladchimescu/microscopy-notebooks.git). Statistical analysis of processed viability and morphological feature data was performed in R and the code is available on Github (https://github.com/vladchimescu/coculture.git).

Results

Imaging-based compound screen in leukemia-stroma coculture

We established a microscopy-based platform (Figure 1) for compound screening in primary blood cancer cells cocultured with the HS-5 bone marrow stromal cell line,[39] which has been demonstrated to reproduce most features of bone marrow–derived stromal cells.[40] Using this platform, we screened 50 compounds at 3 concentrations (supplemental Table 1) in 108 leukemia and lymphoma samples (supplemental Tables 2 and 3) in monoculture and coculture (Figure 1), including CLL (n = 81), AML (n = 17), T-cell prolymphocytic leukemia (n = 4), mantle cell lymphoma (n = 4), and hairy cell leukemia (n = 2). An exposure time of 72 hours and drug concentrations aiming for high, medium, or low toxicity were selected based on a previous internal high-throughput compound screen.[3] After 72 hours, we used Hoechst to stain nuclei in all samples and used confocal microscopy to read out viability and morphological changes in leukemia and lymphoma cells. As previously described, viable CLL cells were identified based on the Hoechst-stained nucleus area[41] (supplemental Figure 1A), whereas in non-CLL entities, an additional staining of the cytoplasm using Calcein was required to distinguish viable and dead cells (supplemental Figure 1B, refer to "Methods" for details). Our primary readout was viability, defined as the viable fraction of leukemia cells. A total of 14 out of 150 drug conditions (50 drugs times 3 concentrations) were identified to be toxic to stromal cells and were thus excluded from further analysis. To adjust for spontaneous apoptosis, viabilities in drug-treated wells were normalized to viabilities in untreated wells. The viability readout of our platform was highly reproducible between replicates with correlations of $R = 0.88$ in coculture and $R = 0.92$ in monoculture (supplemental Figure 1C), and between Hoechst- and Calcein-based readout in CLL samples with correlations of $R = 0.92$ (supplemental Figure 1D).

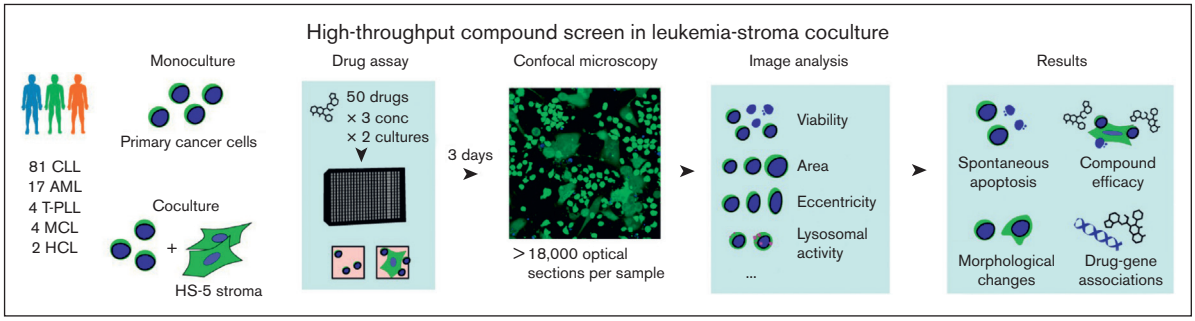

Figure 1. Imaging-based coculture screen in primary leukemias and lymphomas. Study outline. A total of 50 compounds were probed in 108 primary leukemia and lymphoma samples. Confocal microscopy images of leukemia cells alone (in monoculture) and in coculture with the HS-5 stromal cell line were acquired to compute viability and morphological properties.

Degree of stromal protection varies across probed compounds

To assess the degree of spontaneous apoptosis, we determined median raw viability of untreated wells. In monoculture, proportions of viable leukemia cells in the absence of drug treatment were highly variable, ranging from 10% to >90% (supplemental Figure 2). Interestingly, samples with low monoculture viability (<50% alive cells) showed the highest increase in viability in coculture (supplemental Figure 2), reflecting their stronger dependence on the microenvironment signals.

Next, we determined leukemia and lymphoma cell viability after ex vivo exposure to 50 different compounds and compared normalized viabilities in monoculture (supplemental Figure 3) with those in coculture (supplemental Figure 4) using a paired *t* test for each compound. To quantify the effect size of coculture protection, we calculated the difference of the normalized viabilities in coculture and monoculture, and then we normalized it to the mean normalized viability of monoculture (Figure 2A, refer to "Methods" for details). Furthermore, supplemental Figure 5 illustrates the direct comparison between monoculture and coculture viabilities at the single-patient level without additional normalization step (supplemental Figure 6A) summarized for CLL (supplemental Figure 6B) or AML (supplemental Figure 6C). Based on that, we found that 26 out of 50 (=52%) compounds in CLL-stroma coculture and 18 out of 50 (=36%) compounds in AML-stroma coculture were significantly less toxic compared with their corresponding monoculture conditions (Figure 2A; supplemental Table 4). Quantitative assessment of drug efficacy changes in coculture revealed similar patterns in AML and CLL (Figure 2A; supplemental Figure 6). In line with previously reported findings,[19,20,28,42-44] coculture significantly reduced the toxicity of the chemotherapeutics (fludarabine, doxorubicin, cytarabine) both in CLL and AML (Figure 2A). Similarly, the proteasome inhibitors carfilzomib and ixazomib, as well as the Bromodomain and extraterminal domain (BET) inhibitors JQ1 and I-BET-762, showed significantly reduced efficacy in CLL and AML cocultures compared with monocultures (Figure 2A). By coculturing CLL cells with primary MSCs, we reproduced stroma-mediated protection against drug-induced apoptosis using fludarabine as an example (Figure 2B). Unlike HS-5 cells, primary MSCs have not undergone immortalization and were subjected only to a limited time of ex vivo culturing. Similarly, we used primary MSCs to confirm the protection against BET inhibitor–mediated toxicity in CLL (Figure 2C).

In contrast, we identified a considerable proportion of drugs that were similarly effective in CLL (44%) and AML (58%) cocultures (Figure 2A; supplemental Table 4). Among these were both clinically relevant drugs, such as B-cell receptor (BCR)–Abl/Src inhibitor dasatinib, FLT3 inhibitor quizartinib, and cyclin-dependent kinase (CDK) inhibitor palbociclib (Figure 2A), and several experimental compounds, such as Mdm2 inhibitor nutlin 3a, BH3 mimetics obatoclax mesylate and UMI-77, Akt inhibitor MK2206, and NFkB inhibitors EVP4593 and BAY11-7085 (Figure 2A).

These results suggest that the bone marrow microenvironment selectively influences the efficacy of many but not all compounds.

Stroma-leukemia coculture increases toxicity mediated by JAK inhibitors

Among all compounds, only the JAK inhibitors tofacitinib and ruxolitinib were significantly more effective in CLL and AML coculture than in monoculture (Figure 2A). This effect was again confirmed by coculturing CLL cells with primary MSCs and exposing them to ruxolitinib (Figure 3A) and tofacitinib (Figure 3B). Importantly, the JAK-STAT pathway has been suggested as a key mediator of stromal protection.[31,32,45,46] Indeed, we observed that the presence of bone marrow stromal cells increased phosphorylation of STAT3 at Tyr705 in CLL cells, which could be reversed by simultaneous exposure to JAK inhibitors (Figure 3C). Conditioned medium from HS-5 cells or primary MSCs was sufficient to increase STAT3 phosphorylation (Figure 3D), demonstrating that JAK-STAT–mediated protection is based on the exchange of soluble factors. These results highlight the importance of targeting components of the soluble microenvironment for disrupting the interaction between stromal and leukemia cells.

Coculture recapitulates most clinically established drug-gene associations

To identify and compare drug-gene associations between monoculture and coculture, we characterized key genetic features of CLL samples, including TP53 mutation, IGHV status, and trisomy12 status. For each drug-gene pair we performed a *t* test, comparing drug responses in wildtype and mutated groups, as shown for nutlin 3a and TP53 mutation or ibrutinib and IGHV status (Figure 4A). The comparison of the *t* statistic values in monoculture and coculture are summarized in Figure 4B, with significant associations (false discovery rate < 0.1) highlighted. Although the direction of drug-gene associations was preserved in CLL coculture (Figure 4B; supplemental Figure 7), we observed that associations of BCR inhibitors with IGHV and trisomy12 status exhibited smaller effect sizes in CLL coculture than in monoculture (Figure 4C). Consequently, some well-established associations, such as the increased sensitivity of the IGHV-unmutated-CLL (U-CLL) group to ibrutinib,[3,47] could be detected in monoculture but did not reach statistical significance in coculture (Figure 4A; supplemental Table 5). In line with that, we observed that stroma-mediated protection from BCR inhibitors was stronger in IGHV-unmutated-CLL than in IGHV-mutated-CLL (M-CLL) samples (Figure 4D). Furthermore, trisomy12^{+} samples treated with BCR inhibitors were better protected by the stromal microenvironment than trisomy12^{-} samples (Figure 4D).

Coculture reduced not only effect size estimates but also the drug response variability of many compounds, as observed for BCR inhibitors, nutlin 3a, and proteasome inhibitors (Figure 4E). This variance reduction in coculture offset the decrease in effect size and thus enhanced some drug-gene associations, such as higher sensitivity of del11q^{+} samples to proteasome inhibitors (Figure 4B; supplemental Table 5). Despite reduced technical variation, the number of discovered drug-gene associations was higher in monoculture. Thus, monoculture ex vivo drug perturbation studies represent a sensitive first-line screening approach to detect drug-gene associations.

Image-based phenotyping reveals morphological changes upon stromal coculture

Beside Hoechst and Calcein, we stained all samples with a lysosomal dye aiming to obtain information-rich representations describing the morphology of nucleus and cytoplasmic and lysosomal compartments. Then, we segmented cancer cells and extracted and analyzed reproducible morphological properties with

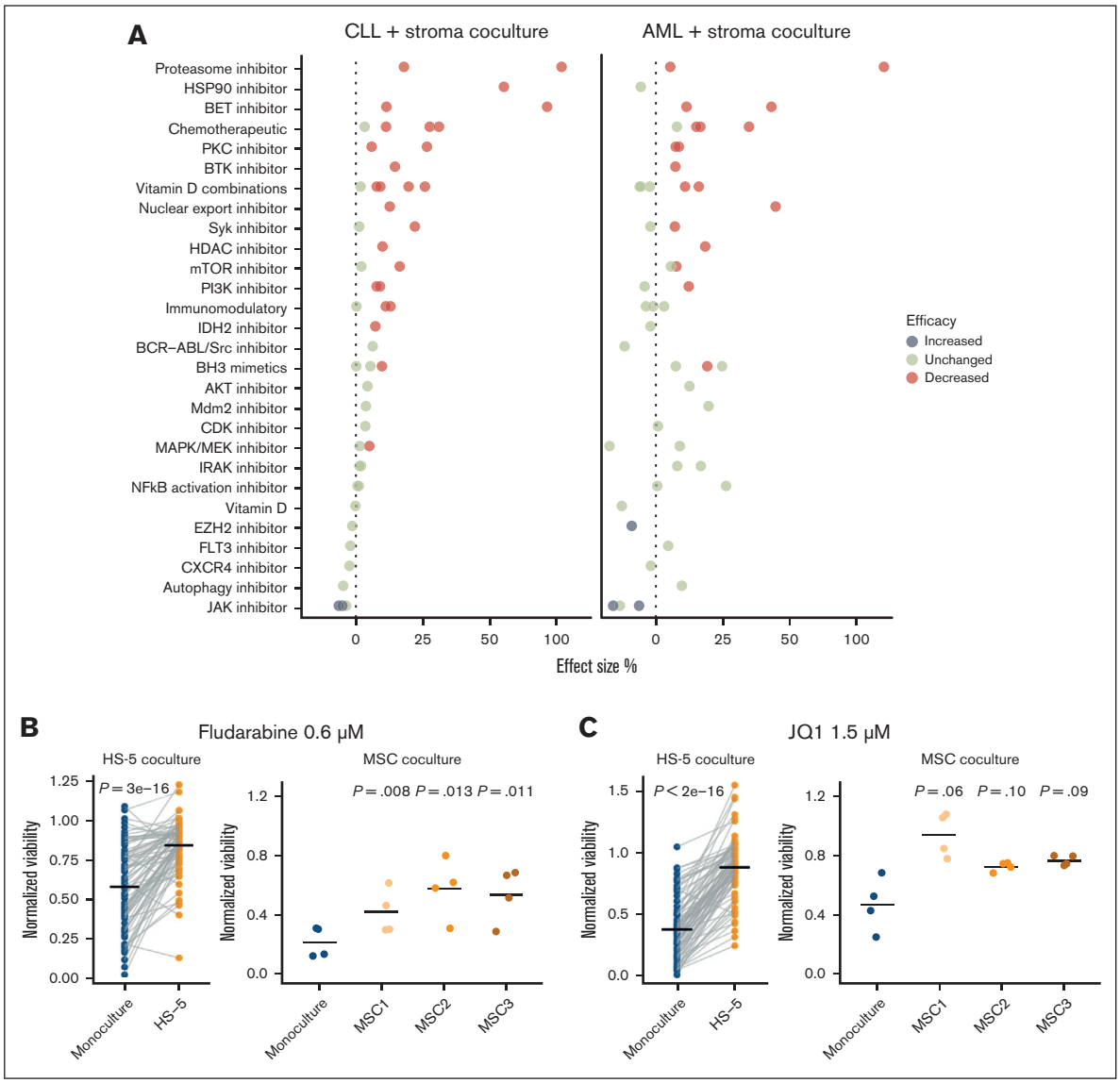

Figure 2. Stroma-mediated modulation of compound efficacy. (A) Shown is the percental drug response change in coculture relative to monoculture (alias effect size) summarized by drug class (refer to "Materials and methods"). An effect size of 100% equals a doubling of the normalized viability in coculture vs monoculture. A *t* test was further used to compare normalized viabilities in coculture vs monoculture. Only differences with a false discovery rate ≤0.01 are highlighted as indicated. A total number of 81 or 17 samples are shown for CLL or AML, respectively. (B-C) Validating the effect of fludarabine 0.6 μM (B) and JQ-1 1.5 μM (C) from the HS-5 coculture screen (n = 81) in cocultures of CLL with primary MSCs (n = 3). *t* tests were used to compare the coculture mean with the reference value in monoculture. MSC1, MSC2, and MSC3 were derived from (n = 3) different healthy donors.

replicate correlations $R > 0.5$ (supplemental Figure 8, refer to "Materials and methods"). First, we investigated the impact of the stromal cells on unperturbed leukemia and lymphoma cells. In AML, a joint t-distributed stochastic neighbor embedding (t-SNE) of viable leukemia cells based on their morphological properties revealed the separation of monoculture and coculture leukemia cell populations (Figure 5A). We found increased Calcein eccentricity and convex area of AML and T-cell prolymphocytic leukemia cells in coculture (Figure 5B; supplemental Figure 9A), suggesting that cells of these disease entities generally take on more elongated shapes in the presence of stromal cells. For B-cell lymphoma and CLL, we did not detect any clear changes in morphology (Figure 5B; supplemental Figure 9B).

Finally, we aggregated viability and morphological features to generate high-dimensional compound profiles of all screened compounds in monoculture and coculture (Figure 5C). Hierarchical clustering recapitulated functional drug classes including BCR inhibitors, immunomodulatory imide drugs, JAK inhibitors, chemotherapeutics, BH3 mimetics, and proteasome inhibitors (Figure 5C). We observed that several drugs displayed higher similarity in monoculture. For instance, although most BCR inhibitors were strongly correlated with one another in both monoculture and coculture, high correlations of sotrastaurin and dasatinib with the other BCR inhibitors were lost in coculture (Figure 5C). JAK inhibitors clustered together, with a high correlation between ruxolitinib and pyridine-6 observed only in monoculture. Similarly, the

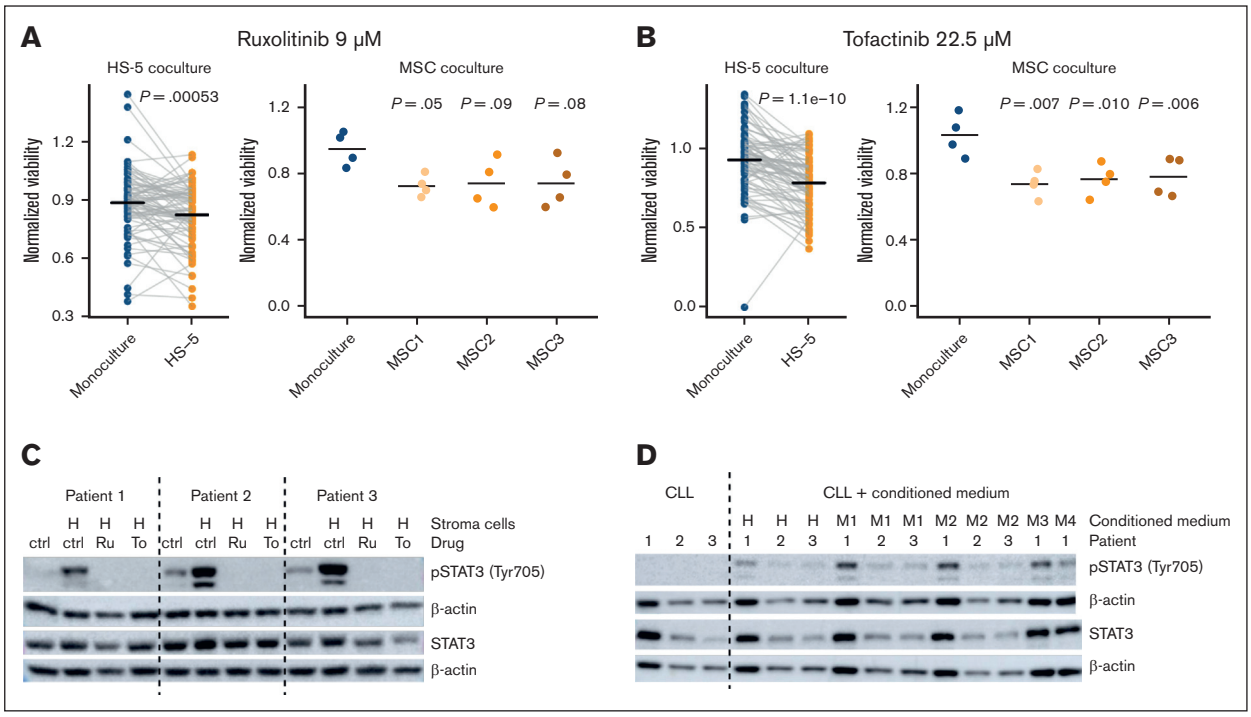

Figure 3. Stroma-leukemia coculture increases toxicity mediated by JAK inhibitors. (A-B) Validating the effects of ruxolitinib (A) tofacitinib (B) from the HS-5 coculture screen (n = 81) in cocultures of CLL with primary MSCs (n = 3). *t* tests were used to compare the coculture mean with the reference value in monoculture. MSC1, MSC2, and MSC3 were derived from n = 3 different healthy donors. (C) STAT3 was phosphorylated in CLL cells from (n = 3) patient samples cocultured with HS-5 cells. STAT3 phosphorylation could be reversed by inhibition with ruxolitinib or tofacitinib. (D) STAT3 was phosphorylated in CLL cells from (n = 3) patient samples in the presence of conditioned medium derived from stromal cells. Ctrl, solvent control (DMSO); H, cocultures with HS-5 cells; M1-4, cocultures with MSC cells from (n = 4) different healthy donors; Ru, ruxolitinib (10 µM); To, tofacitinib (22.5 µM).

profiles of BH3 mimetics, venetoclax, and UMI-77, were more similar in monoculture. The higher within-class heterogeneity observed in coculture suggests that stromal effects may contribute to the varying responses of drugs within the same functional class.

To determine relative importance of microscopy for compound profiling, we compared clustering results based on image features alone and based on viabilities (supplemental Figure 10). This revealed that the BCR inhibitor class could be recapitulated without image features, whereas the clustering of proteasome inhibitors or BH3 mimetics was mainly driven by morphological features (supplemental Figure 10). This suggests that morphological profiling is useful to infer drug mode of action of certain compound classes.

Comparison of monoculture and coculture for microscopy-based screening

Our comprehensive analysis of coculture drug screening has identified both advantages and shortcomings, which we have summarized in Table 1. This list can serve as a guide for future compound screening efforts in hematological malignancies, particularly regarding the applicability of coculture models.

Discussion

In this study, we established a microscopy-based leukemia-stroma coculture platform to systematically evaluate whether coculture models provide superior biological insights compared with that of monoculture studies. Our study found that up to 50% of compounds, including BCR inhibitors, chemotherapeutics, and BET inhibitors, show reduced activity in the presence of bone marrow stromal cells. We observed very similar effects in lymphoid and myeloid malignancies, suggesting a disease-independent mechanism that mediates protection from drug-induced apoptosis. Carfilzomib and bortezomib for instance, 2 proteasome inhibitors, even lost their toxicity in CLL cells almost completely when cocultured with stromal cells. This finding might explain why proteasome inhibitors were clinically ineffective in patients with CLL,[48] thereby underlining the importance of validating drug discoveries in the context of the cancer microenvironment.[19-21,28-35]

Moreover, our study revealed JAK-STAT signaling, and more specifically phosphorylation of STAT3 at Tyr705, as key mediator of stromal protection. Among all the drugs tested, we observed that only JAK inhibitors reduced stroma-mediated protection in lymphoid and myeloid disease entities, thereby confirming findings of previous studies.[31,32,45,46] Although JAK inhibitors alone have low inhibitory activity, they could be used in combination with other clinically established drugs to reduce drug resistance in the bone marrow, which is being evaluated in clinical trials.[49-51] Further clinical applications that overcome stromal protection of leukemia and lymphoma could be revealed by using a more mechanistic readout of apopotois, such as BH3 profiling, instead of the holistic readout of our study.

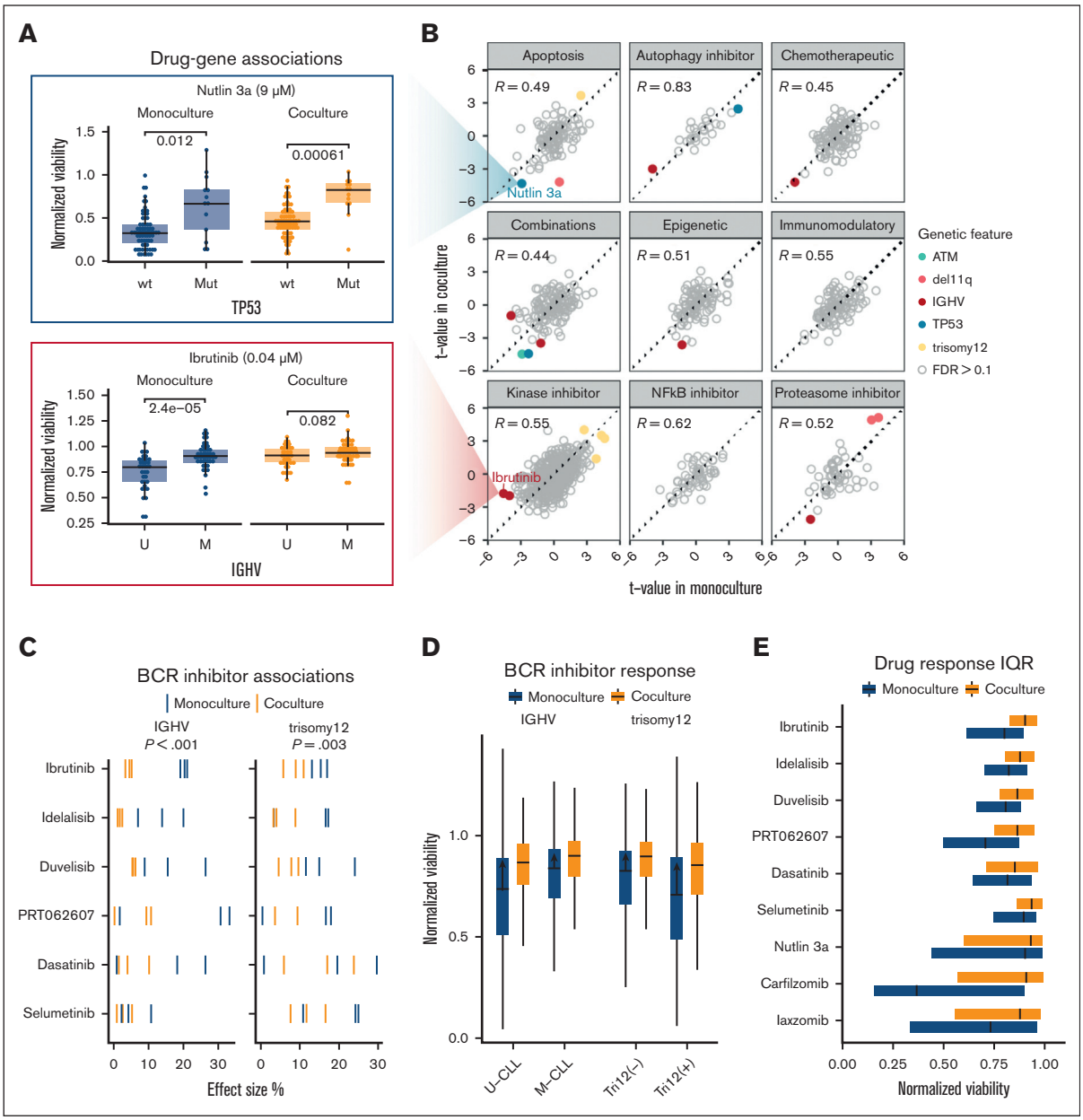

Figure 4. Drug-gene associations in coculture. (A) Boxplots showing response to nutlin 3a and ibrutinib stratified by culture condition and mutational status. (B) Comparison of drug-gene association statistics in monoculture and coculture. The x- and y-axes show the *t* statistic values of drug-gene associations in monoculture and coculture at a given concentration. (C) Effect size of IGHV and trisomy12 associations with BCR inhibitor response. The tick marks, colored by culture condition, show the absolute value of the effect size at 3 probed drug concentrations. Effect sizes of monoculture and coculture were compared using a 1-sided *t* test across all drugs shown. (D) The boxplots, colored by culture condition, show BCR inhibitor response stratified by IGHV mutational status [unmutated-CLL (U-CLL)/mutated-CLL(M-CLL)] and trisomy12 (negative/positive). The arrows indicate differences between monoculture and coculture medians, that is, viability gain in coculture. Monoculture and coculture were compared using a 1-sided *t* test. *P* values of all 4 groups were $<1 \times 10^{-10}$. (E) Drug response variability in CLL samples treated with BCR inhibitors, nutlin 3a, and proteasome inhibitors stratified by culture condition. The boxplots compare the interquartile ranges of drug sensitivities in monoculture and coculture.

To approximate the biological relevance of monoculture and coculture platforms in drug response profiling, we compared well-established associations between genotype and drug response, such as resistance to chemotherapy in patients with mutated *TP53*. Our data not only recapitulated known genotype-drug response associations in CLL, but also demonstrated that most of the identified drug-gene associations were consistent between monoculture and coculture. Importantly, however, the effect sizes of these associations were significantly reduced in coculture. The diversity of in vivo treatments of patients who donated samples for this study did unfortunately not allow a direct correlation of in vivo and ex vivo treatment. Briefly, our study demonstrates that monoculture drug assays represent a superior discovery tool for drug-gene associations because of its lower complexity and higher sensitivity. Co-coculture

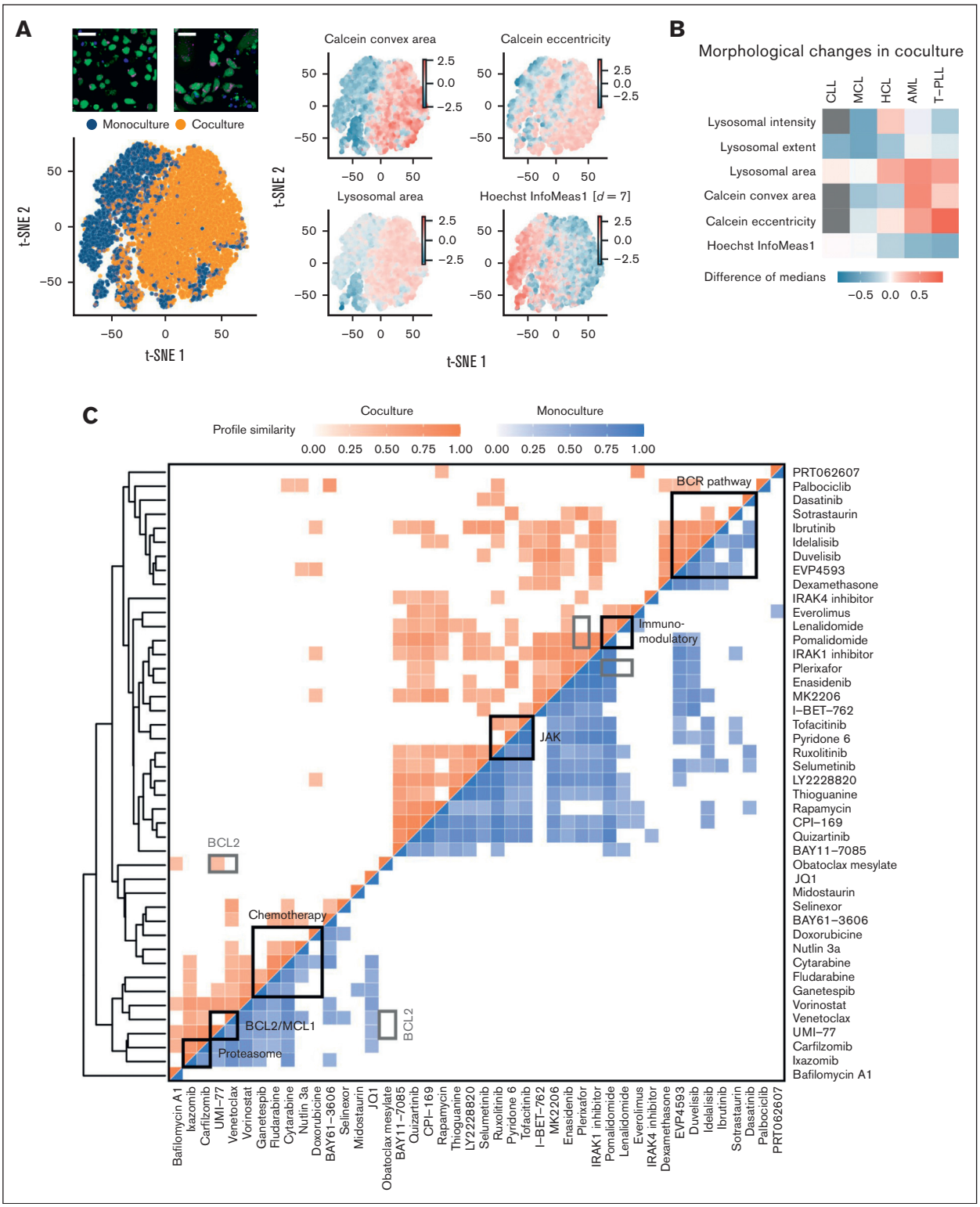

Figure 5. Compound similarity in monoculture and coculture. (A) Joint t-SNE embedding of viable leukemia cells in monoculture and coculture controls of an AML sample. Coloring by morphological features revealed that AML cells in coculture had more elongated shapes (higher eccentricity), larger cell (Calcein), and lysosomal area as well as lower local correlation between pixel intensity values in x- and y-direction (Hoechst InfoMeas1). (B) Heatmap showing morphological changes in coculture controls across all screened disease entities. Gray indicates missing values. (C) Aggregated compound profiles were used to generate a hierarchical clustering of all probed compounds, excluding combinations. Pearson correlation was applied to compare drugs among each other separately in monoculture and coculture. Only high correlations ($r > 0.4$) are indicated in the heatmap. All shown correlations have P values $< .001$. Refer to "Materials and methods" for details.

Table 1. Comparison of mono- and coculture: advantages and challenges

	Monoculture	Coculture
Spontaneous apoptosis	(–) Samples with low viability (<0.25) present a technical challenge	(+) Samples with low viability are rescued from spontaneous apoptosis
Plate-positional effects	(–) Edge effect: edge wells have systematically lower viabilities	(+) No edge effect
Reproducibility	(+) Good correlation ($r = 0.92$)	(+) Good correlation ($r = 0.88$)
Microenvironmental effects	(–) No signals from the microenvironment	(+) Ex vivo model of the bone marrow microenvironment
Drug sensitivity	(+) Drug sensitivity profiles can be used for personalized medicine (citations)	(++) Drug sensitivity profiles in presence of microenvironment signals
Drug-gene associations	(++) Many drug-gene associations are correlated with the clinical outcome	(+) Directions of drug-gene associations preserved. Lower effect size estimates. Variance reduction enhances some associations
Experimental complexity	(+) Easy to handle	(–) More labor-intense
Image analysis	(+) Straightforward	(–) Requires additional staining or machine learning to separate cancer cells from stromal cells

platforms might provide an additional level of confidence of a potential discovery in the context of the tumor microenvironment.

One limitation of our study is the use of a uniform incubation period of 72 hours, which may not be optimal for drugs with different kinetics of toxicity. Although drug-specific adjustments to the incubation period could address this limitation, it would drastically increase the complexity of the coculture screening. Another limitation of our coculture model is the simplifying assumption that the mere presence of bone marrow–derived stromal cells is sufficient to reproduce the tumor microenvironment ex vivo. More complex coculture and organoid systems[52-54] could mitigate some of these limitations, but our work suggests that even simple assays may yield informative drug response phenotypes for the initial assessment of drug efficacy in samples derived from patients.

Acknowledgments

The authors thank all the patients for the donation of cells. T.R. was supported by a fellowship of the German Federal Ministry of Education and Research (BMBF) and a physician scientist fellowship of the Medical Faculty of University Heidelberg. The authors thank Benedikt Brors, Simon Anders, Beate Neumann, Sandrine Sander, Martina Seiffert, Christof von Kalle, and Bernd Fischer for helpful discussions. The authors thank Angela Lenze, Tatjana Walter, Ximing Ding, and Rainer Saffrich for technical support.

The authors gratefully acknowledge the data storage service SDS@hd supported by the Ministry of Science, Research, and the Arts Baden-Württemberg and the German Research Foundation (DFG) through grant INST 35/1314-1 FUGG. S.D. was supported by the Else Kroener Physician Scientist Professorship, Heidelberg Research Centre for Molecular Medicine, an e:med BMBF junior group grant, and Deutsche Forschungsgemeinschaft (DFG). N.L. was supported by a Heidelberg School of Oncology (HSO2) fellowship from the National Center for Tumor Diseases Heidelberg.

Authorship

Contribution: S.A.H. conducted the screening; S.A.H., T.R., P.-M.B., C.K., and M.K. performed validation experiments; V.K. and S.A.H. performed computational analyses; E.C.S. performed data curation; J.L. processed next-generation sequencing data; N.L. collected patient data; P.D., C.M.-T., and T.Z. provided guidance and feedback; S.A.H., V.K., T.R., and S.D. wrote the manuscript; S.A.H., V.K., and T.R. contributed equally to this work; and S.D. and W.H. jointly supervised this work.

Conflict-of-interest disclosure: The authors declare no competing financial interests.

ORCID profiles: S.A.H., 0000-0001-8502-0366; V.K., 0000-0001-5061-7285; T.R., 0000-0002-6973-3531; P.-M.B., 0000-0002-9992-3109; C.M.-T., 0000-0002-7166-5232; W.H., 0000-0002-0474-2218; S.D., 0000-0002-0648-1832.

Correspondence: Sascha Dietrich, Department of Hematology and Oncology, University Hospital Düsseldorf, Moorenstr. 5, 40225 Düsseldorf, Germany; email: sascha.dietrich@embl.de.

References

1. Barretina J, Caponigro G, Stransky N, et al. The Cancer Cell Line Encyclopedia enables predictive modelling of anticancer drug sensitivity. *Nature*. 2012;483(7391):603-607.
2. Garnett MJ, Edelman EJ, Heidorn SJ, et al. Systematic identification of genomic markers of drug sensitivity in cancer cells. *Nature*. 2012;483(7391):570-575.
3. Dietrich S, Oleś M, Lu J, et al. Drug-perturbation-based stratification of blood cancer. *J Clin Invest*. 2018;128(1):427-445.
4. Lu J, Cannizzaro E, Meier-Abt F, et al. Multi-omics reveals clinically relevant proliferative drive associated with mTOR-MYC-OXPHOS activity in chronic lymphocytic leukemia. *Nat Cancer*. 2021;2(8):853-864.

5. Iorio F, Knijnenburg TA, Vis DJ, et al. A landscape of pharmacogenomic interactions in cancer. *Cell*. 2016;166(3):740-754.
6. Basu A, Bodycombe NE, Cheah JH, et al. An interactive resource to identify cancer genetic and lineage dependencies targeted by small molecules. *Cell*. 2013;154(5):1151-1161.
7. Tyner JW, Yang WF, Bankhead A 3rd, et al. Kinase pathway dependence in primary human leukemias determined by rapid inhibitor screening. *Cancer Res*. 2013;73(1):285-296.
8. Pemovska T, Kontro M, Yadav B, et al. Individualized systems medicine strategy to tailor treatments for patients with chemorefractory acute myeloid leukemia. *Cancer Discov*. 2013;3(12):1416-1429.
9. Roider T, Seufert J, Uvarovskii A, et al. Dissecting intratumour heterogeneity of nodal B-cell lymphomas at the transcriptional, genetic and drug-response levels. *Nat Cell Biol*. 2020;22(7):896-906.
10. Roider T, Brinkmann BJ, Kim V, et al. An autologous culture model of nodal B-cell lymphoma identifies ex vivo determinants of response to bispecific antibodies. *Blood Adv*. 2021;5(23):5060-5071.
11. Snijder B, Vladimer GI, Krall N, et al. Image-based ex-vivo drug screening for patients with aggressive haematological malignancies: interim results from a single-arm, open-label, pilot study. *Lancet Haematol*. 2017;4(12):e595-e606.
12. Kornauth C, Pemovska T, Vladimer GI, et al. Functional precision medicine provides clinical benefit in advanced aggressive hematologic cancers and identifies exceptional responders. *Cancer Discov*. 2022;12(2):372-387.
13. Collins RJ, Verschuer LA, Harmon BV, Prentice RL, Pope JH, Kerr JF. Spontaneous programmed death (apoptosis) of B-chronic lymphocytic leukaemia cells following their culture in vitro. *Br J Haematol*. 1989;71(3):343-350.
14. Bendall LJ, Daniel A, Kortlepel K, Gottlieb DJ. Bone marrow adherent layers inhibit apoptosis of acute myeloid leukemia cells. *Exp Hematol*. 1994; 22(13):1252-1260.
15. Bergfeld SA, Blavier L, DeClerck YA. Bone marrow-derived mesenchymal stromal cells promote survival and drug resistance in tumor cells. *Mol Cancer Ther*. 2014;13(4):962-975.
16. Schulz A, Toedt G, Zenz T, Stilgenbauer S, Lichter P, Seiffert M. Inflammatory cytokines and signaling pathways are associated with survival of primary chronic lymphocytic leukemia cells in vitro: a dominant role of CCL2. *Haematologica*. 2011;96(3):408-416.
17. Bruch PM, Giles HA, Kolb C, et al. Drug-microenvironment perturbations reveal resistance mechanisms and prognostic subgroups in CLL. *Mol Syst Biol*. 2022;18(8):e10855.
18. Dubois N, Crompot E, Meuleman N, Bron D, Lagneaux L, Stamatopoulos B. Importance of crosstalk between chronic lymphocytic leukemia cells and the stromal microenvironment: direct contact, soluble factors, and extracellular vesicles. *Front Oncol*. 2020;10:1422.
19. Konopleva M, Konoplev S, Hu W, Zaritskey AY, Afanasiev BV, Andreeff M. Stromal cells prevent apoptosis of AML cells by up-regulation of anti-apoptotic proteins. *Leukemia*. 2002;16(9):1713-1724.
20. Kurtova AV, Balakrishnan K, Chen R, et al. Diverse marrow stromal cells protect CLL cells from spontaneous and drug-induced apoptosis: development of a reliable and reproducible system to assess stromal cell adhesion-mediated drug resistance. *Blood*. 2009;114(20):4441-4450.
21. Panayiotidis P, Jones D, Ganeshaguru K, Foroni L, Hoffbrand AV. Human bone marrow stromal cells prevent apoptosis and support the survival of chronic lymphocytic leukaemia cells in vitro. *Br J Haematol*. 1996;92(1):97-103.
22. Lagneaux L, Delforge A, Bron D, De Bruyn C, Stryckmans P. Chronic lymphocytic leukemic B cells but not normal B cells are rescued from apoptosis by contact with normal bone marrow stromal cells. *Blood*. 1998;91(7):2387-2396.
23. Burger JA, O'Brien S. Evolution of CLL treatment - from chemoimmunotherapy to targeted and individualized therapy. *Nat Rev Clin Oncol*. 2018;15(8): 510-527.
24. Ten Hacken E, Burger JA. Microenvironment interactions and B-cell receptor signaling in chronic lymphocytic leukemia: implications for disease pathogenesis and treatment. *Biochim Biophys Acta*. 2016;1863(3):401-413.
25. Moffat JG, Rudolph J, Bailey D. Phenotypic screening in cancer drug discovery - past, present and future. *Nat Rev Drug Discov*. 2014;13(8):588-602.
26. Horvath P, Aulner N, Bickle M, et al. Screening out irrelevant cell-based models of disease. *Nat Rev Drug Discov*. 2016;15(11):751-769.
27. Cucchi DGJ, Groen RWJ, Janssen JJWM, Cloos J. Ex vivo cultures and drug testing of primary acute myeloid leukemia samples: current techniques and implications for experimental design and outcome. *Drug Resist Updat*. 2020;53:100730.
28. Mudry RE, Fortney JE, York T, Hall BM, Gibson LF. Stromal cells regulate survival of B-lineage leukemic cells during chemotherapy. *Blood*. 2000;96(5): 1926-1932.
29. Vianello F, Villanova F, Tisato V, et al. Bone marrow mesenchymal stromal cells non-selectively protect chronic myeloid leukemia cells from imatinib-induced apoptosis via the CXCR4/CXCL12 axis. *Haematologica*. 2010;95(7):1081-1089.
30. Nwabo Kamdje AH, Bassi G, Pacelli L, et al. Role of stromal cell-mediated Notch signaling in CLL resistance to chemotherapy. *Blood Cancer J*. 2012; 2(5):e73.
31. Quintarelli C, De Angelis B, Errichiello S, et al. Selective strong synergism of ruxolitinib and second generation tyrosine kinase inhibitors to overcome bone marrow stroma related drug resistance in chronic myelogenous leukemia. *Leuk Res*. 2014;38(2):236-242.
32. Karjalainen R, Pemovska T, Popa M, et al. JAK1/2 and BCL2 inhibitors synergize to counteract bone marrow stromal cell-induced protection of AML. *Blood*. 2017;130(6):789-802.

33. Zhang X, Tu H, Yang Y, et al. Bone marrow-derived mesenchymal stromal cells promote resistance to tyrosine kinase inhibitors in chronic myeloid leukemia via the IL-7/JAK1/STAT5 pathway. *J Biol Chem*. 2019;294(32):12167-12179.
34. Zeng Z, Shi YX, Samudio IJ, et al. Targeting the leukemia microenvironment by CXCR4 inhibition overcomes resistance to kinase inhibitors and chemotherapy in AML. *Blood*. 2009;113(24):6215-6224.
35. Gupta SV, Hertlein E, Lu Y, et al. The proteasome inhibitor carfilzomib functions independently of p53 to induce cytotoxicity and an atypical NF-kappaB response in chronic lymphocytic leukemia cells. *Clin Cancer Res*. 2013;19(9):2406-2419.
36. Szankasi P, Bahler DW. Clinical laboratory analysis of immunoglobulin heavy chain variable region genes for chronic lymphocytic leukemia prognosis. *J Mol Diagn*. 2010;12(2):244-249.
37. Ren S, He K, Faster R-CNN, Girshick R, Sun J. Faster R-CNN: towards real-time object detection with region proposal networks. *IEEE Trans Pattern Anal Mach Intell*. 2017;39(6):1137-1149.
38. Szegedy C, Liu W, Jia Y, et al. Going deeper with convolutions. Paper presented at: 2015 IEEE Conference on Computer Vision and Pattern Recognition (CVPR). 7-12 June 2015. Boston, MA.
39. Roecklein BA, Torok-Storb B. Functionally distinct human marrow stromal cell lines immortalized by transduction with the human papilloma virus E6/E7 genes. *Blood*. 1995;85(4):997-1005.
40. Adamo A, Delfino P, Gatti A, et al. HS-5 and HS-27A stromal cell lines to study bone marrow mesenchymal stromal cell-mediated support to cancer development. *Front Cell Dev Biol*. 2020;8:584232.
41. Crowley LC, Marfell BJ, Waterhouse NJ. Analyzing cell death by nuclear staining with hoechst 33342. *Cold Spring Harb Protoc*. 2016;2016(9). pdb.prot087205.
42. Kay NE, Shanafelt TD, Strege AK, Lee YK, Bone ND, Raza A. Bone biopsy derived marrow stromal elements rescue chronic lymphocytic leukemia B-cells from spontaneous and drug induced cell death and facilitates an "angiogenic switch". *Leuk Res*. 2007;31(7):899-906.
43. Mraz M, Zent CS, Church AK, et al. Bone marrow stromal cells protect lymphoma B-cells from rituximab-induced apoptosis and targeting integrin alpha-4-beta-1 (VLA-4) with natalizumab can overcome this resistance. *Br J Haematol*. 2011;155(1):53-64.
44. Zhang W, Trachootham D, Liu J, et al. Stromal control of cystine metabolism promotes cancer cell survival in chronic lymphocytic leukaemia. *Nat Cell Biol*. 2012;14(3):276-286.
45. Severin F, Frezzato F, Visentin A, et al. In chronic lymphocytic leukemia the JAK2/STAT3 pathway is constitutively activated and its inhibition leads to CLL cell death unaffected by the protective bone marrow microenvironment. *Cancers*. 2019;11(12):1939.
46. Weisberg E, Liu Q, Nelson E, et al. Using combination therapy to override stromal-mediated chemoresistance in mutant FLT3-positive AML: synergism between FLT3 inhibitors, dasatinib/multi-targeted inhibitors and JAK inhibitors. *Leukemia*. 2012;26(10):2233-2244.
47. Guo A, Lu P, Galanina N, et al. Heightened BTK-dependent cell proliferation in unmutated chronic lymphocytic leukemia confers increased sensitivity to ibrutinib. *Oncotarget*. 2016;7(4):4598-4610.
48. Faderl S, Rai K, Gribben J, et al. Phase II study of single-agent bortezomib for the treatment of patients with fludarabine-refractory B-cell chronic lymphocytic leukemia. *Cancer*. 2006;107(5):916-924.
49. Oppermann S, Lam AJ, Tung S, et al. Janus and PI3-kinases mediate glucocorticoid resistance in activated chronic leukemia cells. *Oncotarget*. 2016;7(45):72608-72621.
50. Spaner DE, Wang G, McCaw L, et al. Activity of the Janus kinase inhibitor ruxolitinib in chronic lymphocytic leukemia: results of a phase II trial. *Haematologica*. 2016;101(5):e192-e195.
51. Spaner DE, McCaw L, Wang G, Tsui H, Shi Y. Persistent janus kinase-signaling in chronic lymphocytic leukemia patients on ibrutinib: results of a phase I trial. *Cancer Med*. 2019;8(4):1540-1550.
52. Bleijs M, van de Wetering M, Clevers H, Drost J. Xenograft and organoid model systems in cancer research. *EMBO J*. 2019;38(15):e101654.
53. Gava F, Pignolet J, Déjean S, et al. 3D model characterization by 2D and 3D imaging in t(14;18)-positive B-NHL: perspectives for in vitro drug screens in follicular lymphoma. *Cancers*. 2021;13(22):5840.
54. Ham IH, Oh HJ, Jin H, et al. Targeting interleukin-6 as a strategy to overcome stroma-induced resistance to chemotherapy in gastric cancer. *Mol Cancer*. 2019;18(1):68.